Mechanically superior matrices promote osteointegration and regeneration of anterior cruciate ligament tissue in rabbits

Paulos Y. Mengsteab[a,b,c], Takayoshi Otsuka[a,b], Aneesah McClinton[a,b,d], Nikoo Saveh Shemshaki[a,b,c], Shiv Shah[a,b,e], Ho-Man Kan[a,b], Elifho Obopilwe[f], Anthony T. Vella[g], Lakshmi S. Nair[a,b,c,f,h], and Cato T. Laurencin[a,b,c,e,f,h,i,1]

[a]Connecticut Convergence Institute for Translation in Regenerative Engineering, University of Connecticut Health, Farmington, CT 06030; [b]Raymond and Beverly Sackler Center for Biological, Physical and Engineering Sciences, University of Connecticut Health, Farmington, CT 06030; [c]Department of Biomedical Engineering, University of Connecticut, Storrs, CT 06269; [d]Department of Surgery, University of Connecticut School of Medicine, Farmington, CT, 06030; [e]Department of Chemical and Biomolecular Engineering, University of Connecticut, Storrs, CT 06269; [f]Department of Orthopedic Surgery, University of Connecticut Health, Farmington, CT 06030; [g]Department of Immunology, University of Connecticut School of Medicine, Farmington, CT 06030; [h]Department of Materials Science and Engineering, University of Connecticut, Storrs, CT 06269; and [i]Department of Reconstructive Sciences, University of Connecticut Health Center, Farmington, CT 06030

Edited by Robert Langer, Massachusetts Institute of Technology, Cambridge, MA, and approved September 21, 2020 (received for review June 19, 2020)

The gold standard treatment for anterior cruciate ligament (ACL) reconstruction is the use of tendon autografts and allografts. Limiting factors for this treatment include donor site morbidity, potential disease transmission, and variable graft quality. To address these limitations, we previously developed an off-the-shelf alternative, a poly(L-lactic) acid (PLLA) bioengineered ACL matrix, and demonstrated its feasibility to regenerate ACL tissue. This study aims to 1) accelerate the rate of regeneration using the bioengineered ACL matrix by supplementation with bone marrow aspirate concentrate (BMAC) and growth factors (BMP-2, FGF-2, and FGF-8) and 2) increase matrix strength retention. Histological evaluation showed robust tissue regeneration in all groups. The presence of cuboidal cells reminiscent of ACL fibroblasts and chondrocytes surrounded by an extracellular matrix rich in anionic macromolecules was upregulated in the BMAC group. This was not observed in previous studies and is indicative of enhanced regeneration. Additionally, intraarticular treatment with FGF-2 and FGF-8 was found to suppress joint inflammation. To increase matrix strength retention, we incorporated nondegradable fibers, polyethylene terephthalate (PET), into the PLLA bioengineered ACL matrix to fabricate a "tiger graft." The tiger graft demonstrated the greatest peak loads among the experimental groups and the highest to date in a rabbit model. Moreover, the tiger graft showed superior osteointegration, making it an ideal bioengineered ACL matrix. The results of this study illustrate the beneficial effect bioactive factors and PET incorporation have on ACL regeneration and signal a promising step toward the clinical translation of a functional bioengineered ACL matrix.

PLLA | BMAC | ACL | tendon | osteointegration

The goal of developing a bioengineered anterior cruciate ligament (ACL) matrix is to provide an off-the-shelf product that is functionally superior to autografts and allografts currently used for ACL reconstruction surgeries. There is clear need for advancement in this area as 30% of young active patients reinjure their ACL after surgery (1). Furthermore, athletes in the National Basketball Association and National Football League have a return-to-sport time after ACL reconstruction of 11.6 and 10.8 mo, respectively (2, 3). This lengthy period of rehabilitation has spurred interest in bioengineered ACL matrices that can accelerate and enhance ACL regeneration, so that all patients can return to their preinjury performance level faster.

Our group previously fabricated a poly(L-lactic) acid (PLLA) bioengineered ACL matrix and evaluated its performance in rabbit ACL reconstruction models (4–7). The bioengineered ACL matrix resulted in excellent tissue regeneration, while experiencing a 41 to 66% rupture rate in vivo (4, 5). The cause of these ruptures was likely due to the interplay between the rate of tissue regeneration and matrix fatigue. Thus, this study aims to 1) accelerate ACL regeneration by supplementing the bioengineered ACL matrix with bone marrow aspirate concentrate (BMAC) and growth factors (bone morphogenetic protein 2 [BMP-2], fibroblast growth factor 2 [FGF-2], and FGF-8); and 2) increase the strength retention of the bioengineered ACL matrix by incorporating nondegradable polyethylene terephthalate (PET) yarns.

BMAC is a promising translational stem cell therapy as it can be harvested and applied during surgery and is not regulated by the US Food and Drug Administration (FDA) (8, 9). The ability of BMAC to enhance the repair of damaged rotator cuff (10) and meniscus (11) tissues has been demonstrated in rabbit models. Thus, we hypothesized that the application of BMAC would serve as a source of progenitor cells and bioactive factors that would accelerate ACL regeneration. This report evaluates the feasibility of obtaining BMAC in a rabbit ACL reconstruction model and its regenerative potential.

Significance

This paper describes a mechanically superior matrix that enhances the osteointegration and regeneration of ACL tissue in a rabbit model. We show that bone marrow aspirate concentrate enhances the presence of cuboidal cells that are reminiscent of ACL fibroblasts and chondrocytes, a sign of enhanced regeneration. This paper also demonstrates that the combinatorial application of FGF-2 and FGF-8 in the knee joint suppresses inflammation by reducing adipokine secretion. The incorporation of nondegradable PET fibers into the PLLA bioengineered ACL matrix showed improved strength retention after implantation. We report the strongest matrix to date in a rabbit ACL reconstruction model, which is a promising step toward the clinical translation of an off-the-shelf ligament for orthopedic applications.

Author contributions: P.Y.M., L.S.N., and C.T.L. designed research; P.Y.M., T.O., A.M., N.S., S.S., H.-M.K., and E.O. performed research; P.Y.M., T.O., N.S., S.S., A.T.V., L.S.N., and C.T.L. analyzed data; and P.Y.M., T.O., L.S.N., and C.T.L. wrote the paper.

Competing interest statement: C.T.L. has the following competing financial interests: Biorez, Globus, HOT, HOT Bone, Kuros Bioscience, NPD, and Cobb (W. Montague) NMA Health Institute. L.S.N. has the following competing financial interests: Biorez.

This article is a PNAS Direct Submission.

[1]To whom correspondence may be addressed. Email: laurencin@uchc.edu.

This article contains supporting information online at https://www.pnas.org/lookup/suppl/doi:10.1073/pnas.2012347117/-/DCSupplemental.

First published November 3, 2020.

Growth factors have been widely investigated to accelerate bone and ligament regeneration through the proliferation and differentiation of progenitor cells (12). FGFs have been shown to stimulate the proliferation of cells and enhance tissue healing. In particular, FGF-2 has been shown to accelerate ligament healing (13), and a member of the FGF-8 subfamily has been shown to stimulate cartilage healing in a clinical study (14). Furthermore, the synergistic application of FGF-2 and FGF-8 induced dedifferentiation of mature cells in axolotls (15). Given the evidence supporting the proregenerative qualities of FGF-2 and FGF-8, we chose to apply FGF-2 and FGF-8 simultaneously in the intraarticular space. We hypothesized that the combinatorial application of FGF-2 and FGF-8 would accelerate ligamentization of the bioengineered ACL matrix by promoting the proliferation of progenitor cells and dedifferentiation of mature cells in the synovial environment.

To accelerate bone regeneration, we utilized bone morphogenetic protein 2 (BMP-2), which is approved by the US FDA for a range of lumbar spinal fusion procedures and has been shown in ACL reconstruction models to enhance osteointegration of tendon grafts (16–18). In our previous study, we demonstrated that BMP-2 saline injections could enhance osteoid seam width and reduce bone tunnel cross-sectional area, a sign of bone regeneration (5). However, the effect was limited, likely due to the lack of a drug carrier. In this study, we hypothesized that the addition of a drug delivery carrier, fibrin glue (19–22), would potentiate the effect of BMP-2 and promote bone formation (23).

The first iteration of the bioengineered ACL matrix, termed the "L-C ligament," was completely biodegradable and composed of only PLLA yarns (4). The high rupture rate found in our previous study motivated us to modify the material composition of the bioengineered ACL matrix to reduce its mechanical fatigue rate. A compelling polymer to reduce fatigue rate is PET, a biocompatible nondegradable polymer with high tensile strength that has previously been utilized for orthopedic applications (24). To date, no study has investigated the use of a composite PLLA and PET bioengineered ACL matrix for ACL reconstruction. Following the patented design by Laurencin and colleagues (25), a composite bioengineered ACL matrix, termed the "tiger graft," composed of 20 PLLA yarns and 4 PET yarns, was fabricated. The PLLA facilitates a greater volume of tissue regeneration as it gradually degrades, while the PET bolsters the mechanical strength of the matrix during the early phases of healing. We hypothesized that the tiger graft would have increased mechanical strength retention over the implantation period.

The overall goal of this study was to accelerate ACL regeneration of a bioengineered ACL matrix by supplementation with BMAC and growth factors (BMP-2, FGF-2, and FGF-8) and by modulating the material composition of the matrix (Fig. 1). We evaluated the ligamentization and osteointegration of the bioengineered ACL matrices histologically. Microcomputed tomography (μCT) was performed to evaluate bone tunnel regeneration. The inflammatory and remodeling state of the synovial fluid was evaluated using an enzyme-linked immunosorbent assay (ELISA). Finally, biomechanical testing was conducted to determine the strength retention of the bioengineered ACL matrices.

Results

Intraoperative Processing of Bone Marrow Aspirate Yields a Concentrated Cell Population. Bone marrow aspirate (BMA) was isolated from the femur and tibia of each rabbit in the BMAC treatment group (Fig. 2*A* and Movie S1). Approximately 6 mL of bone marrow was isolated from the femur and tibia in total. Fig. 2*B* demonstrates a representative image of a bone marrow cast after isolation. Subsequently the BMA was centrifuged, and the presence of a buffy coat was observed (Fig. 2 *C* and *D*). A blood smear of isolated BMA was prepared, and a Giemsa stain was conducted to analyze the constituent cells. The presence of megakaryocytes in the blood smear was indicative of cells from the bone marrow niche (Fig. 2*E*, red arrow). During bone marrow isolation, contamination with peripheral blood could not be avoided and was undoubtedly present in the BMA. Flow cytometry was utilized to characterize the cell count and viability before (BMA) and after centrifugation (BMAC) (Fig. 2 *F* and *G*). Nucleated cell viability was increased in the BMAC group in comparison to BMA (Fig. 2*H*; $^{**}P = 0.0059$, Wilcoxon test). Furthermore, the number of total nucleated cells was quantified using an equal volume of BMA and BMAC. It was found that BMAC yielded a 2.37-fold increase in total nucleated cells in comparison to BMA (Fig. 2*I*; $^{**}P = 0.0020$, Wilcoxon test). BMAC was plated and cultured in vitro for 14 d and stained with crystal violet to count colonies. Fig. 2*J* demonstrates a colony of >50 cells, which is counted as one colony. All BMAC cultures resulted in colony formation (mean colony-forming units ± SD [range], 13 ± 7 [7 to 22]) (Fig. 2*K*).

Ninety-Five Percent of the Bioengineered ACL Matrices Were Intact at 12 wk. The majority of the bioengineered ACL matrices maintained their integrity at 12- and 24-wk post-ACL reconstruction ($n = 54$). At 12 wk, rabbits were weight-bearing with limping noted in some cases. At the time of harvest, loss of knee extension in the operated knees was typically observed. Overall, the knee joints were devoid of the gross appearance of cartilage degeneration and the margins of tissue structures were well observed (Fig. 3*A*). In some cases, fibrosis of the knee joint was seen. For the L-C ligament, one rabbit had a fibrotic knee joint, and one rabbit presented with a dislocated patella and fibrosis of the knee joint. In the L-C ligament with BMAC therapy group, one rabbit had a damaged posterior cruciate ligament at the time of surgery and was removed from the study. In the L-C ligament with growth factors therapy group, three joints were found to be fibrotic. One case of fibrosis was documented for the L-C Ligaments that were implanted for 24 wk. Three of 11 tiger grafts displayed fibrotic knee joints. Of the 44 bioengineered ACL matrices implanted for 12 wk, 95.35% were documented to be intact at the time of harvest, and no statistical difference between groups was found (Fig. 3*B*). At 24 wk, 63.64% of the L-C Ligaments ($n = 11$) were intact.

Femoral and Tibial Bone Tunnels Demonstrate a Similar Regeneration Pattern. Histological analysis of the bone tunnels was conducted to evaluate the pattern of regeneration. Fig. 3*C* shows the presence of the microfibers in the bone tunnel and the general maintenance of the braided morphology of the bioengineered ACL matrix at 12 wk. The birefringence of the PLLA and PET microfibers allowed for their visualization under polarized microscopy. Overall, tissue regeneration within the bone tunnels of the femur and tibia was similar. Cell populations consisting of classical fibroblast morphology were present along with a distinct population of (cubodial cells). In general, the bone tunnel area was not found to consist of mineralized collagen (Fig. 3 *D* and *E*), but the presence of anionic macromolecules was observed (Fig. 3 *F* and *G*).

Progressive Bone Regeneration through Endochondral Ossification Is Seen in the L-C Ligament Group at 24 wk. We next investigated whether bone regeneration would progress in the bone tunnel from the 12- to 24-wk time point. The L-C ligament was implanted for 24 wk and histological analysis was carried out. More mature osteointegration of the graft was found with the presence of PLLA fibers embedded in mineralized collagen at 24 wk (Fig. 4*A*). Cells were embedded in the mineralized collagen, indicating that the tissue was alive at harvest and not an artifact of histological processing. Furthermore, bone regeneration within the bone tunnel proper was observed with mineralized collagen once again being accompanied by the presence of cells (Fig. 4*B*). The histological analysis suggests that bone regeneration progressed from 12 to 24 wk.

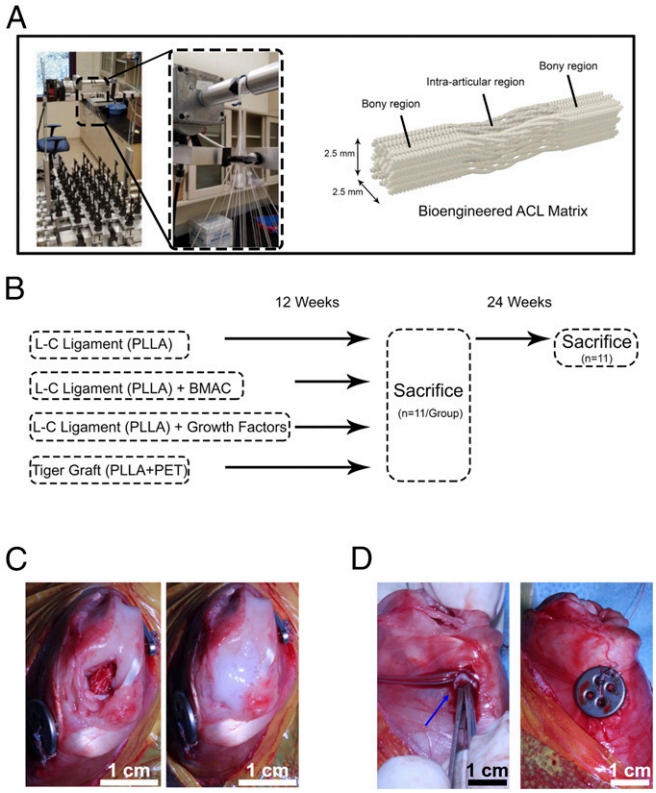

Fig. 1. Fabrication of the bioengineered ACL matrix and implantation in a rabbit ACL reconstruction model. (*A*) Depiction of the braiding machine used to fabricate the bioengineered ACL matrices and the resulting biphasic structure of the matrix. Each matrix was composed of 24 yarns. (*B*) For the L-C ligament, 24 yarns of PLLA were braided together. For the tiger graft, 20 yarns of PLLA and 4 yarns of PET were braided together. Experimental groups were evaluated at 12 wk, and the L-C ligament (control) was further evaluated at 24 wk. (*C*) View of implanted bioengineered ACL matrix at the time of surgery (*Left*) and the application of fibrin glue (*Right*). BMAC or growth factors were mixed with fibrin glue for the experimental groups. (*D*) Representative image demonstrating the implantation of a fibrin gel in the tibial bone tunnel (*Left*, blue arrow) and subsequent fixation of a titanium suture button (*Right*).

To gain insight into the mechanism of bone regeneration, we analyzed the cell morphology and matrix composition at 12 and 24 wk with histological staining. Higher magnification of the bone tunnel proper at 12 wk revealed a columnar arrangement of cubodial cells between the PLLA fibers of the bioengineered ACL matrix (Fig. 4*C*, navy arrows). At 24 wk, a similar columnar arrangement of cells was seen (Fig. 4*C*, navy arrow). However, cell size had decreased, and the matrix contained mineralized collagen. To further analyze the composition of the matrix, two cationic dyes were employed, toluidine blue and Safranin O. Metachromasia of both dyes was observed around cubodial cells, indicating the aggregation of the basic dyes in an anionic region (Fig. 4*D*, yellow arrows and *SI Appendix*, Fig. 1). Given the arrangement of cells between the fibers of the bioengineered ACL matrix, we hypothesized that cells between the fibers were subjected to compressive forces while the graft was in tension (Fig. 4*E*). The progression of bone regeneration observed suggests an endochondral ossification mechanism may be involved.

BMAC Treatment Alters the Cellular Phenotype of Regenerated Tissue. The enthesis, bone tunnel proper, and bioengineered ACL matrix–bone interface regions were analyzed to determine the effect of biological cues and material properties on bone tunnel regeneration. At the enthesis a mixture of azophloxine (red dye) and Orange G (orange dye) staining was seen (Fig. 5 *A*, *i*, green boxes). In some cases, cellular detail could be distinguished and cubodial cells were observed (Fig. 5 *A*, *i*). This was most clear in the tiger graft group, where columnar arrangements of cubodial cells were seen (Fig. 5 *A*, *i*). Orange G staining was more prevalent at the enthesis in the L-C ligament + BMAC treatment and tiger graft groups (Fig. 5 *A*, *i*).

Next, the regeneration of the bone tunnel proper was evaluated for cell populations based on morphology and density. The bone tunnel proper was defined as the area distal to the aperture and not immediately adjacent to trabecular bone (Fig. 5 *A*, *ii*). A greater number of cubodial cells accompanied with greater Orange G staining was observed in the bone tunnel proper in the L-C ligament + BMAC treatment group. Cell density was found to be qualitatively similar among groups. Toluidine blue staining was used to assess the presence of proteoglycans and chondrocytes in the bone tunnel (*SI Appendix*, Fig. S1). Semiquantitative analysis demonstrated that BMAC-treated groups had significantly greater areas of metachromasia (areas with proteoglycans or chondrocytes) in the femur in comparison to the L-C ligament alone (Fig. 5*B*, one-way ANOVA with Dunnett's post hoc test). A trend toward greater metachromasia was seen in the tibia for the BMAC group as well, but this was not significant (Fig. 5*C* one-way ANOVA with Dunnett's post hoc test). These results suggest that BMAC therapy may affect the cell populations present in the bone tunnel proper.

Finally, we assessed the osteointegration of the bioengineered ACL matrices at 12 wk. Indirect osteointegration, with the presence of Sharpey's fibers, was found for the L-C ligament (Fig. 5 *A*, *iii*). Treatment with BMAC resulted in limited direct osteointegration as PLLA fibers were found to be embedded in mineralized collagen (Fig. 5 *A*, *iii*). Additionally, the presence of cuboidal cells at the matrix–bone interface was observed. Treatment with growth factors resulted in robust direct osteointegration with a multitude of PLLA fibers embedded in mineralized collagen in one case (Fig. 5 *A*, *iii*).

Intraarticular Treatment with FGF-2 and FGF-8 Down-Regulates Inflammation. We evaluated the effect of the various treatments on the inflammatory state of the intraarticular microenvironment. This was achieved by isolating the synovial fluid at the time of harvest and analyzing the cytokine composition through a multiplex ELISA. Fig. 6*A* shows a heat map of the cytokine levels represented as the log of normalized means, such that a value of zero indicates that the cytokine means are equivalent to the L-C ligament. Positive and negative values indicate up-regulation and down-regulation, respectively. Treatment with FGF-2 and FGF-8 (growth factors group) resulted in an increased occurrence of purple to blue shades on the heat map, which demonstrates down-regulation of cytokine levels. Of the 20 cytokines assayed, 7 were found to reach statistical significance between the L-C ligament group and the growth factors group (Fig. 6 *B*–*H*, Kruskal–Wallis test). Overall, it was found that treatment with FGF-2 and FGF-8 resulted in reduced production of proinflammatory cytokines (e.g., IL-1a, IL-8, MIP-1b, and Leptin) (Fig. 6 *B*, *C*, *E*, and *F*) (26, 27). Interestingly, FGF-2 and FGF-8 treatment also resulted in up-regulation of the antiinflammatory cytokine IL-1RA in the synovial fluid (Fig. 6*H*) (28). However, it was also found that FGF-2 and FGF-8 treatment resulted in a reduced presence of IL-13, another antiinflammatory cytokine, in the synovial fluid (Fig. 6*D*) (28). We further analyzed the correlation between Leptin production and the other cytokines. We found a strong positive correlation between Leptin and proinflammatory cytokines, such as MIP-1b (Fig. 6*I* and *SI Appendix*, Fig. S3). Moreover, we found a negative correlation between Leptin and IL-1RA, an antiinflammatory cytokine (Fig. 6*J*). Additionally, principal-component analysis was conducted, and it was found that

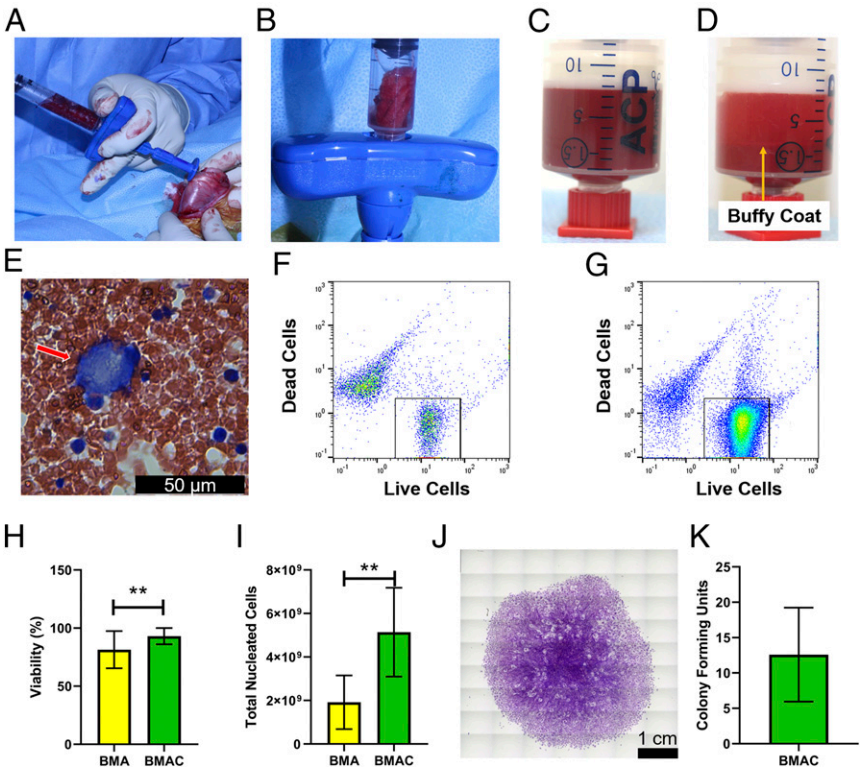

Fig. 2. Intraoperative processing of BMA yields a concentrated cell population. (*A*) Representative image of bone marrow aspiration (BMA) isolation from the femur. (*B*) Representative image of a bone marrow cast after intraoperative BMA. (*C*) BMA before centrifugation. (*D*) Representation of buffy coat (orange arrow) after centrifugation of BMA. (*E*) Representative Giemsa staining of BMA demonstrating presence of a megakaryocyte (red arrow). (*F*) Representative flow cytometry plot of live and dead cells before centrifugation and (*G*) after centrifugation. (*H*) Cell viability percentage for BMA and bone marrow aspirate concentrate (BMAC). Mean cell viability percentage ± SD (n = 10; 1 outlier removed); $^{**}P$ = 0.0059, Wilcoxon test. (*I*) Total nucleated cell counts for BMA and BMAC. Mean total nucleated cells ± SD (n = 11); $^{**}P$ = 0.0020, Wilcoxon test. (*J*) Representative image of crystal violet staining of BMAC 14 d post seeding (n = 5). (*K*) Quantification of colony-forming units at day 14 post seeding of BMAC (n = 5).

the L-C ligament + growth factors group separated from the L-C ligament alone (*SI Appendix*, Fig. S4). This cytokine analysis suggests that FGF-2 and FGF-8 treatment reduced intraarticular inflammation at 12 wk.

We hypothesized that intraarticular inflammation would subside over time. At 24 wk, the proinflammatory cytokines IL-1a and IL-8 were significantly reduced in comparison to 12 wk (Fig. 6 *B* and *C*). Principal-component analysis also revealed that the L-C ligament cytokine data at 12 and 24 wk were distinct from each other (*SI Appendix*, Fig. S4). Additionally, the presence of the proinflammatory cytokines MIP-1b and Leptin trended down at 24 wk (Fig. 6 *E* and *F*). However, the antiinflammatory cytokine IL-13 was found to be significantly reduced at 24 wk as well (Fig. 6*D*). Overall, the data suggest that the intraarticular microenvironment was less inflamed at 24 wk.

Incorporation of PET Fibers in the Bioengineered ACL Matrix Enhances Osteointegration and Decreases Bone Tunnel Cross-Sectional Area via Increased Mineral Apposition Rate. Histological and μCT imaging demonstrated that the incorporation of PET fibers into the tiger graft resulted in enhanced osteointegration. Goldner's Trichrome staining of the tiger graft revealed that fibers were embedded in mineralized collagen at the bioengineered ACL matrix–bone interface (Fig. 5 *A*, *iii*). To gain further insight into the osteointegration of the matrices, we conducted μCT imaging. Representative μCT three-dimensional (3D) reconstructions demonstrated the gross appearance of the fibrin glue implantation sites in the femur and tibia (Fig. 7 *A* and *B*). In the femur, partial bone bridging at the extracortical site was seen in most samples; however, complete resolution of the bone tunnel defect caused by ACL reconstruction was not observed. Furthermore, BMP-2 treatment (growth factors group) was found to have more extensive bone bridging. The cross-sectional area was measured at discrete locations along the bone tunnel (intraarticular aperture, midtunnel, and extracortical aperture). As the bone tunnel moved distally, from the intraarticular space, a trend toward reduced cross-sectional area was observed (Fig. 7*C*, one-way ANOVA with Dunnett's post hoc test). No differences between groups were seen at the extracortical aperture. In the midtunnel, a trend toward reduced cross-sectional area was observed for the tiger graft group. Growth factors treatment also demonstrated a trend toward reduced bone tunnel cross-sectional area at the intraarticular aperture. Furthermore, a significant reduction in cross-sectional area was seen in the tiger graft group compared with the L-C ligament.

μCT 3D reconstructions of the tibia demonstrated that the growth factors treatment resulted in closure of the extracortical aperture in some cases (Fig. 7*B*). Overall, the extracortical aperture of the tibia demonstrated more resolved healing than the femur. However, tibial bone tunnel cross-sectional area was not found to be significantly altered by the various treatments (Fig. 7*D*, one-way ANOVA with Dunnett's post hoc test). The mineral apposition rate was measured to assess the biological activity of osteoblasts between treatment groups. Representative images of areas used for the measurement of the femoral and tibial bone tunnel are shown in *SI Appendix*, Fig. S5 *A* and *B*. It was found that the tiger graft had enhanced mineral apposition rate in the femur at the posterior midtunnel region (Fig. 7*E*, one-way ANOVA with Dunnett's post hoc test). The results from the Goldner's Trichrome staining, μCT imaging, and mineral apposition rate analysis suggest that the incorporation of PET fibers in the tiger graft group enhanced bone regeneration.

L-C Ligament and Tiger Graft Have Nearly Identical Tensile Properties. Mechanical testing was conducted to determine the differences in tensile properties between the L-C ligament and tiger graft. The bioengineered ACL matrices were fabricated by a 3D braiding machine and were composed of a bony and intraarticular region (Fig. 1*A*) (5, 29). The L-C ligament and tiger graft had identical dimensions 2.5 × 2.5 × 3.54 mm (width × height × diagonal). Furthermore, the tensile properties of the L-C ligament and tiger graft were nearly identical (*SI Appendix*, Fig. S6*A*). The mean peak load of the L-C ligament and tiger graft were 977 ± 28 and

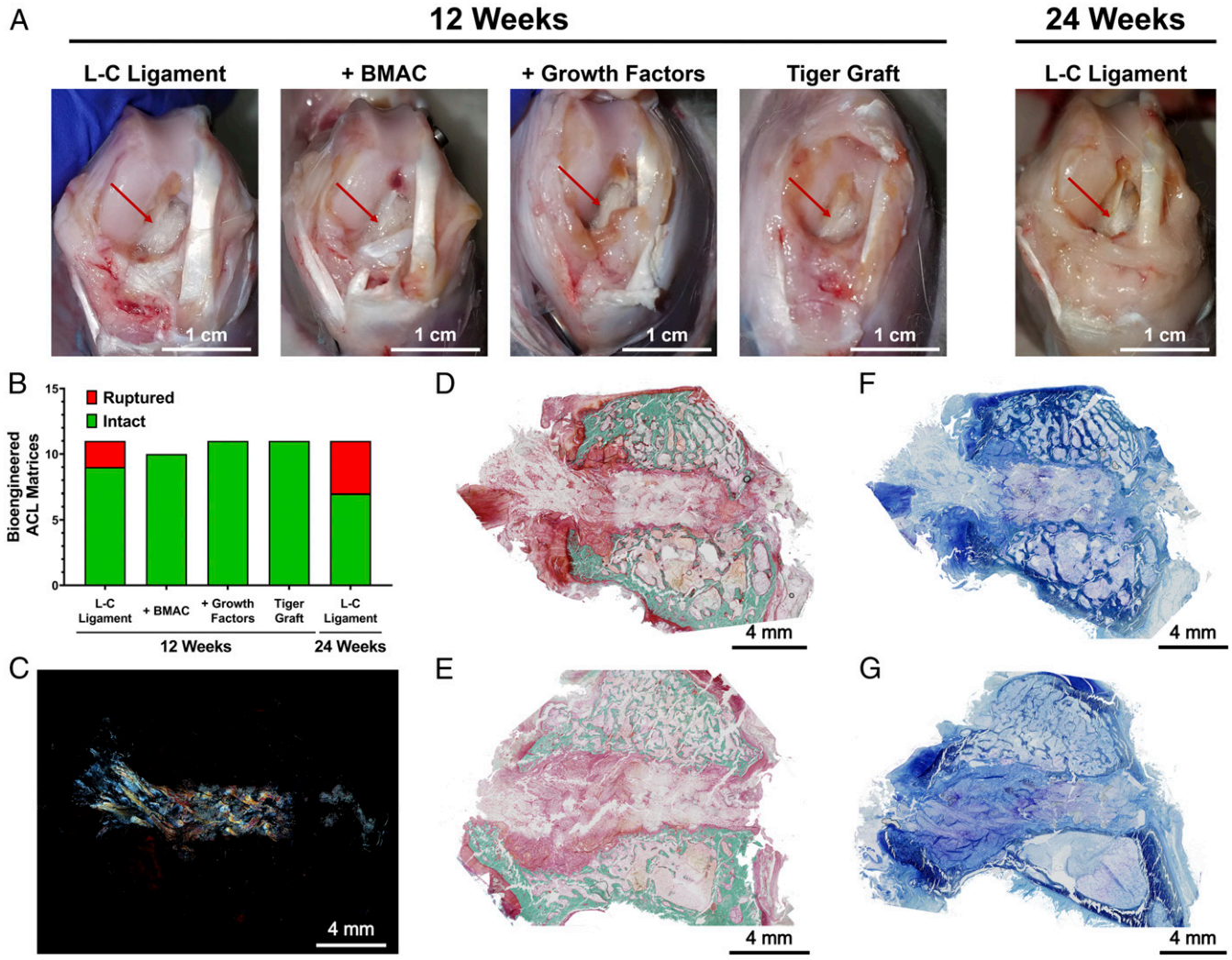

Fig. 3. Ninety-five percent of the bioengineered ACL matrices were intact at 12 wk. (*A*) Representative images of knee joint and bioengineered ACL matrices (red arrow) in each group at 12 and 24 wk. (Scale bars, 1 cm.) (*B*) Assessment of gross state of bioengineered ligaments at 12 and 24 wk ($n = 11$; one BMAC sample excluded due to surgical complication); no significant difference between groups, Fisher's exact test. (*C*) Polarized microscopy image demonstrates presence of braided bioengineered ligament within the bone tunnel. (*D*) Same histological section as *C* stained with Goldner's tichrome staining. Representative Goldners Trichrome staining of (*D*) femoral and (*E*) tibial bone tunnel at 12 wk ($n = 3$; green, mineralized bone; scarlet, osteoid; red, soft tissue). (Scale bars, 4 mm.) Representative toluidine blue staining of (*F*) femoral and (*G*) tibial bone tunnels ($n = 3$; metachromatic staining, purple). (Scale bars, 4 mm.)

993 ± 16 N, respectively ($P = 0.4175$, Mann–Whitney test, *SI Appendix*, Fig. S6*B*). The stiffness was 32 ± 4 and 33 ± 3 N/mm for the L-C ligament and tiger graft, respectively ($P = 0.3602$, unpaired t test; *SI Appendix*, Fig. S6*C*). The length of the toe region was 12.36 ± 0.60 and 14.84 ± 1.52 mm for the L-C ligament and tiger graft, respectively, with no significant difference ($P = 0.058$, unpaired t test; *SI Appendix*, Fig. S6*D*). We were able to compare the fatigue of the L-C ligament and tiger graft as their initial mechanical properties were similar.

Incorporation of PET Fibers into the Bioengineered ACL Matrix Resulted in Enhanced Mechanical Properties at 12 wk Comparable to the Native Rabbit ACL. Tensile tests of the femur-bioengineered ACL matrix–tibia complex were performed to gain insight into the functional effects of treatment (*SI Appendix*, Fig. S7*A*). The femur-bioengineered ACL matrix–tibia complex was loaded to failure, and three modes of failure were found: 1) primary midsubstance rupture (*SI Appendix*, Fig. S6*B*); 2) bone tunnel pull-out from either the femur or tibia, but not both (*SI Appendix*, Fig. S7*C*); or 3) bone tunnel pull-out from both femoral and tibial bone tunnels (*SI Appendix*, Fig. S7*D*). In the case of failure mode 2 and 3, further mechanical tests were performed to measure the strength of osteointegration and functionality of the bioengineered ACL matrices.

The sutures during tensile testing were preserved to determine the weakest link of the femur-bioengineered ACL matrix–tibia complex. In some cases, tensile tests resulted in primary midsubstance rupture. Of these bioengineered ACL matrices, the tiger graft demonstrated a trend toward greater peak loads (Fig. 8*A*). The stiffness of the L-C ligament with growth factors treatment and tiger graft were comparable, and they were greater than other groups at 12 wk. This demonstrated that the bioengineered ACL matrix was the weakest link of the graft at 12 wk in the case of primary midsubstance rupture.

Failure mode 2 was the criteria we used to determine the strength of osteointegration at the bioengineered ACL matrix–bone interface (*SI Appendix*, Fig. S7*C*). Closer examination of *SI Appendix*, Fig. S7*C* shows that the fiberloop (blue suture) is present in the intraarticular space and indicates that suture fixation was stronger than osteointegration. In these cases, the suture was subsequently removed, and the free end of the bioengineered

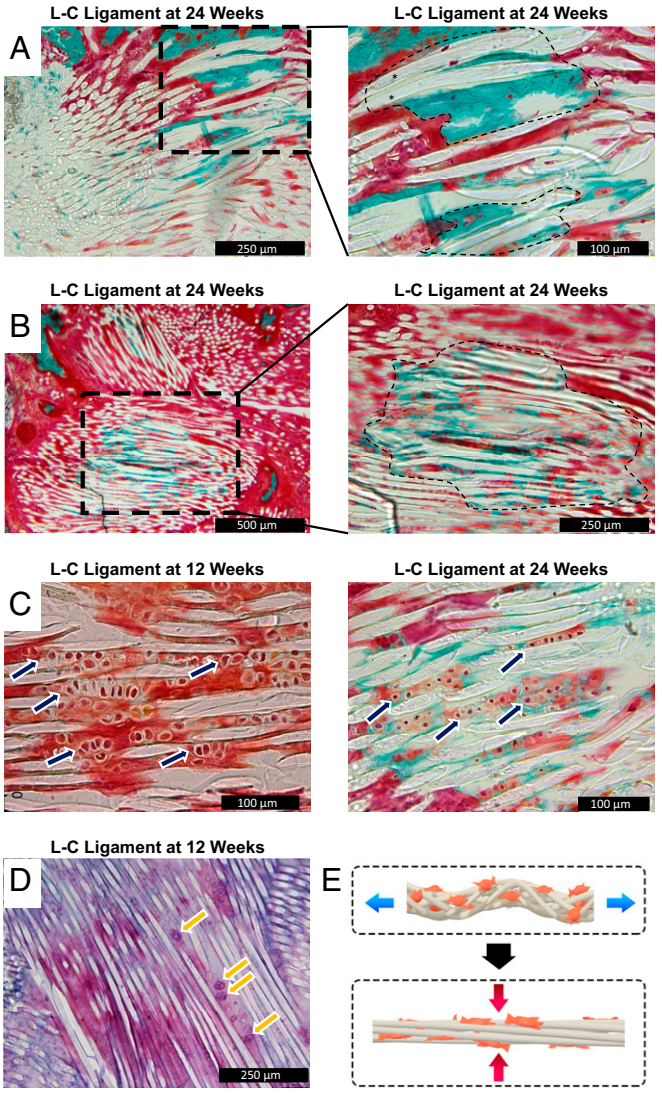

Fig. 4. Progressive bone regeneration through endochondral ossification is seen in the L-C ligament group at 24 wk. (*A*) Representative image of the bioengineered ACL matrix–bone interface (n = 3, 24 wk post-ACL reconstruction). The black outlined box indicates area of higher magnification. The black outlined area represents areas with PLLA fibers embedded in mineralized bone. (*B*) Representative image of the L-C ligament in the bone tunnel proper (n = 3, 24 wk post-ACL reconstruction). The black outlined box indicates area of higher magnification. The black outlined area represents areas with PLLA fibers embedded in mineralized bone. (*C*) Representative image of the L-C ligament at 12 and 24 wk (n = 3). The navy arrows denote areas with columnar arrangement of cuboidal cells. (*D*) Representative Safranin O/azophloxin staining of the L-C ligament. The yellow arrows point to cuboidal cells with metachromasia staining. (*E*) Schematic of mechanical forces placed on bioengineered ACL matrix.

ACL matrix clamped and loaded to failure. Of the samples tested, the tiger graft group trended toward greater pull-out loads and stiffness (Fig. 8*B*). This suggests that the incorporation of PET in the tiger graft may allow for greater osteointegration, which is consistent with our histological observation (Fig. 5 *A*, *iii*).

We next sought to determine the tensile properties of the bioengineered ACL matrices alone to determine their functionality. Tests were performed on bioengineered ACL matrices after the osteointegration test (*SI Appendix*, Fig. S7*C*), or after failure mode 3 (*SI Appendix*, Fig. S7*D*). The bioengineered ACL matrices were loaded in tension to failure. Midsubstance ruptures were the primary mode of rupture (n = 16/19) (*SI Appendix*, Fig. S7 *D*, *Right*), and a few jaw-break failures were also observed (n = 3/19). The tiger graft trended toward greater peak loads in comparison to other groups at 12 wk and was comparable to the native rabbit ACLs (Fig. 8*C*). The L-C ligament + BMAC was the only group found to have a significantly reduced peak load in comparison to the native rabbit ACL (Fig. 8*C*, one-way ANOVA with Dunnett's post hoc test). Treatment of the L-C ligament + BMAC and growth factors trended toward enhanced stiffness, and the stiffness of the tiger graft was comparable to the growth factor treatment group. Of note, the stiffness of the native rabbit ACL was comparable to all treatment groups. The peak load of the L-C ligament was found to be sharply reduced at 24 wk, and the small sample size also represents the higher number of ruptures at that time point. Overall, the results suggest that the bioengineered ACL matrices were mechanically competent at 12 wk.

Discussion

This study investigated the effects of biological factors and material composition on the regeneration and functional outcomes of a bioengineered ACL matrix. Through histological and biomechanical analysis, we observed that the combination of PLLA and PET (tiger graft) improved the osteointegration and mechanical strength of the bioengineered ACL matrix. BMAC was found to enhance the presence of cuboidal cells and an extracellular matrix rich in anionic macromolecules. Interestingly, growth factor treatment (FGF-2 and FGF-8 in intraarticular space) was found to significantly reduce the presence of proinflammatory cytokines in the synovial fluid. Of the 54 ACL reconstructions performed, 95.35% of the bioengineered ACL matrices were intact at 12 wk, a 29–54% improvement over previous studies conducted by our group; this is likely owed to the improved surgical technique (*SI Appendix*, Fig. S8 and Movie S2) (4, 5). Furthermore, the secondary midsubstance peak loads of the bioengineered ACL matrices were >300 N, three times the strength of tendon grafts used in comparable studies (30, 31). These results have led to the generation of several hypotheses regarding the beneficial role of PET fibers, BMAC, and growth factors in the function and regeneration of a bioengineered ACL matrix.

Structural Differences Between Tendon Grafts and Bioengineered ACL Matrices May Contribute to the Different Cellular Phenotypes Observed in the Bone Tunnel. The bioengineered ACL matrix was designed to have an interconnected macroporous structure conducive to cell infiltration (32). The macroporous structure of the bioengineered ACL matrix constitutes the main structural difference from the dense solid structure of tendon grafts (32, 33). Unlike tendon grafts, the porosity of the bioengineered ACL matrix allows for blood from the bone marrow to infiltrate the central region of the matrix at the time of surgery. Tendon autografts and allografts may lack the appropriate pore size to allow for progenitor cells to infiltrate, which may explain why cuboidal cells have been confined to the bone–tendon graft interface in bone tunnel healing models (20, 34). Studies suggest that the natural tendon–bone healing process after ACL reconstruction also fails to regenerate bone throughout the bone tunnel and to stimulate the proliferation of cuboidal cells throughout the thickness of the tendon within the bone tunnel proper (35, 36). Furthermore, a recent study showed that synthetic ligaments and hamstring tendon autografts do not fully regenerate the bone within the bone tunnel when examined at 10 y post-ACL reconstruction with radiographic and MRI assessments (37).

Further examination of the morphology and order of the cuboidal cells seen in our study revealed a columnar arrangement oriented parallel to the length of the matrix fibers. Interestingly, this finding is consistent with the histologic appearance of ACL fibroblasts and hypertrophic chondrocytes (Figs. 4*C* and 5 *A*, *i* and *ii*) (38). Cuboidal cells were surrounded by a highly anionic

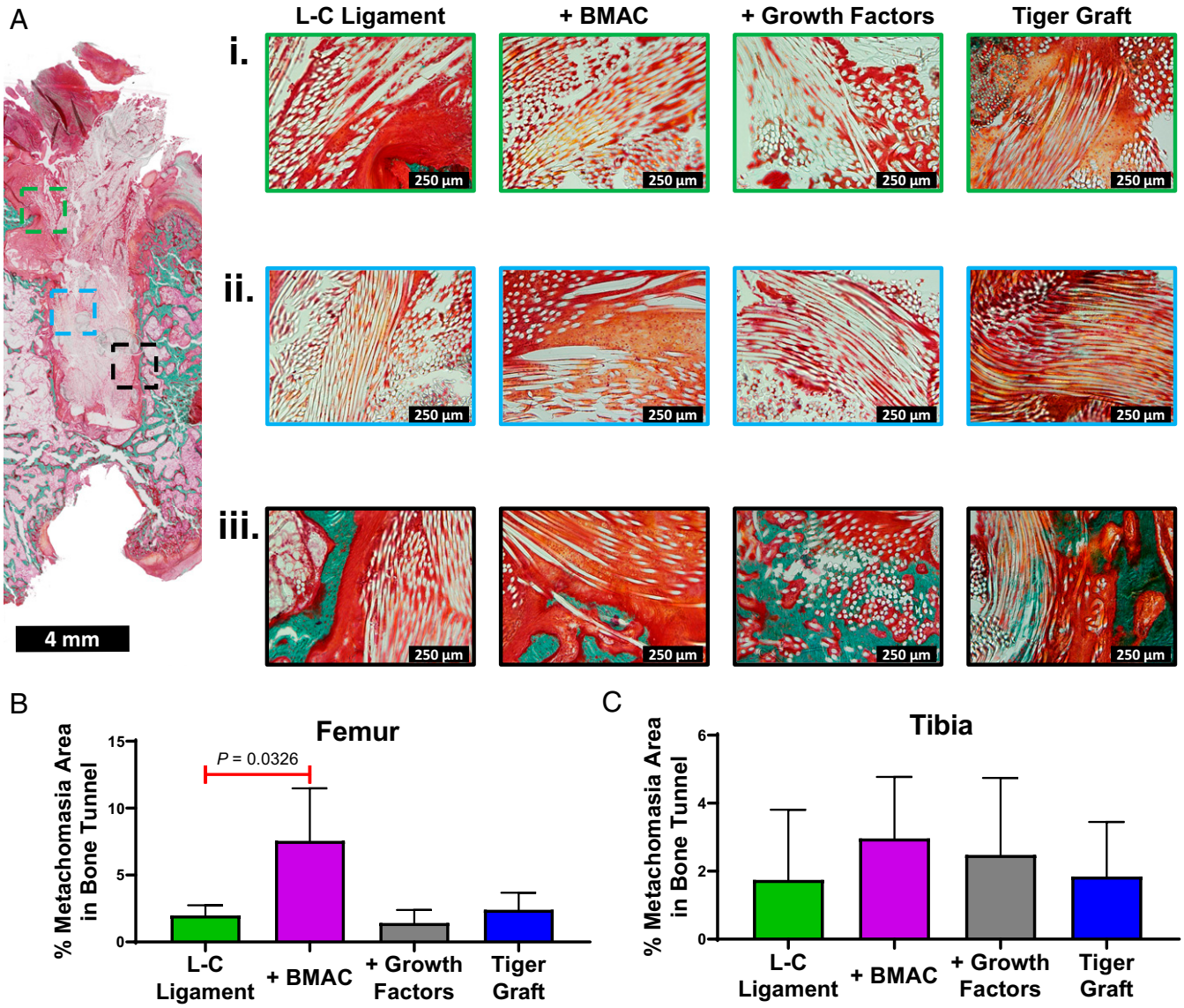

Fig. 5. BMAC as well as growth factor treatment alter the cellular phenotype of regenerated tissue. (*A*) Representative Goldner's Trichrome staining of the femur for the L-C ligament (n = 3, 12 wk post ACL reconstruction). The outlined boxes indicate area of higher magnification. The outlined boxes are color coded (green, enthesis area; light blue, bone tunnel proper; black, ligament–bone interface). Representative higher-magnification images of the (*i*) enthesis (*ii*) bone tunnel proper, and (*iii*) bioengineered ACL matrix–bone interface area for the L-C ligament, L-C ligament + BMAC treatment, L-C ligament + growth factors treatment, and tiger graft. The image of the entire bone tunnel length for the treatment groups can be found in *SI Appendix*, Fig. S2. (*B* and *C*) Area of metachromasia was quantified as a percentage of the bone tunnel area for toluidine blue stains in the femur and tibia. Mean area of metachromasia ± SD (n = 3, 12 wk post-ACL reconstruction); one-way ANOVA with Dunnett's post hoc test.

extracellular matrix as shown through metachromasia of toluidine blue and Safranin O stains (Fig. 4*D* and *SI Appendix*, Fig. S1). Similar staining has been found in histology sections of the distal native ACL, which is cartilaginous (39). In our design of a bioengineered ACL matrix, we aimed for complete regeneration, and the presence of cuboidal cells represents an encouraging step toward the regeneration of the ligament proper and the potential for stimulating the regeneration of bone through endochondral ossification.

Compressive Forces May Contribute to the Observed Cuboidal Cellular Morphology. There is a body of literature that suggests that compressive forces stimulate chondrogenesis (40). Although the primary force placed on the bioengineered ACL matrix was tension, it has been established that compressive forces are also placed on the yarns of a braided matrix when it is loaded in tension (Fig. 4*E*) (41). The bioengineered ACL matrix was designed to incorporate a greater braiding angle in the bony region to facilitate larger pore sizes conducive to bone regeneration. This also resulted in greater compressive forces exerted on the yarns in the bony region (Fig. 4*E*). In our previous study, there was a high rupture rate of the matrices and cuboidal cells were not present in the bone tunnel proper (5). We concluded that the high rupture rate was likely due to excessive pretension of the matrices caused by a more anterior tibial bone tunnel placement and matrix fixation at full knee extension. We hypothesize that the presence of cuboidal cells may be due to consistent mechanical loading of the bioengineered ACL matrix, which occurred in this study due to the high success rate.

The bioengineered ACL matrix was designed to mimic the size of collagen fibers seen in the native ACL. This structural similarity is thought to facilitate the generation of physical forces on

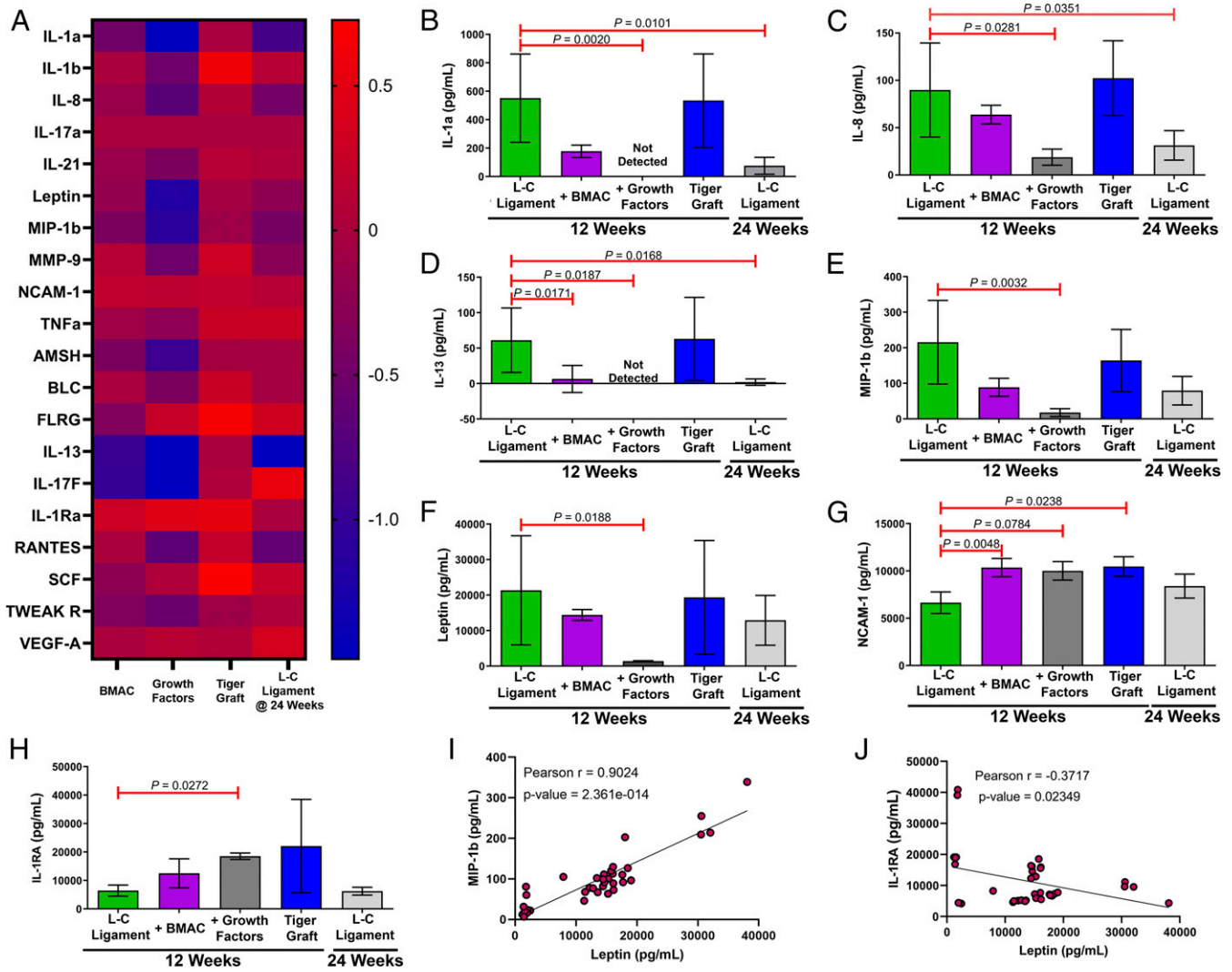

Fig. 6. Intraarticular treatment with FGF-2 and FGF-8 down-regulates inflammation. (*A*) Heat map of cytokine levels normalized to the L-C ligament at 12 wk (control). Data are the log of the normalized mean. (*B–H*) Quantification of a multiplex cytokine antibody array. Data are mean ± SD ($n = 3$ to 11). *P* values are indicated in each panel; Kruskal–Wallis test (nonparametric one-way ANOVA) with Dunn's multiple-comparisons test with L-C ligament as the control. (*I* and *J*) Correlation plot of Leptin vs. macrophage inflammatory protein 1 (MIP-1b) and interleukin-1 receptor antagonist (IL-1RA) (*xy* pairs = 37). Pearson correlation analysis.

cells that are like those seen during fibrocartilage formation at the enthesis (42). Through electron microscopy studies, it was demonstrated that collagen fibers surround cuboidal cells in a figure-eight fashion at the enthesis and cause compressive forces when loaded in tension (43). Pauwels (44) first described the theory of "causal histogenesis," which posits that the compressive forces on mesenchymal cells by tensioned collagen fibers leads to chondroid cell transformation (cuboidal cells). Our hypothesis, based on the lack of mechanical loading in the previous study, is consistent with Pauwels' theory that mechanical forces contribute to a chondroid cell transformation (44). Future studies should further investigate the role of controlled mechanical loading on the presence of cuboidal cells within the bioengineered ACL matrix.

BMAC May Serve as a Source of Progenitor Cells or a Reservoir of Trophic Factors for Tissue Regeneration. BMAC therapy increased the number of cuboidal cells seen, which suggests that BMAC may have provided a source of progenitor cells and/or bioactive factors that contributed to the cuboidal phenotype observed. However, we could not discern whether the shift in cellular phenotype arose primarily from 1) the differentiation of the injected stem cells, 2) the secretion of trophic factors from the injected stem cells, or 3) a change in the microenvironment due to the bioactive factors present in the BMAC. A few studies have investigated the survival of implanted mesenchymal stem cells (MSCs) (45, 46). MSCs survived up to 8 mo in one study (46). However, these studies were unable to determine whether the implanted stem cells differentiated. Aside from differentiation, implanted stem cells also have trophic activity, which involves the secretion of bioactive factors that promote a regenerative microenvironment (47). Finally, BMAC is also rich in growth factors and cytokines that can contribute to angiogenesis, chondrogenesis, and MSC-homing (48). Therefore, future studies should explore the feasibility of intraoperative labeling of BMAC and subsequent cell lineage tracing to determine whether the observed increase of cuboidal cells arose from the injected stem cells, trophic factors, and/or bioactive factors in the BMAC.

BMAC is a clinically relevant biologic, yet there are few clinical studies that have investigated the use of BMAC to enhance ACL regeneration. Centeno et al. (49) reported upon a case series in which patients were treated with intraligamentous injection of

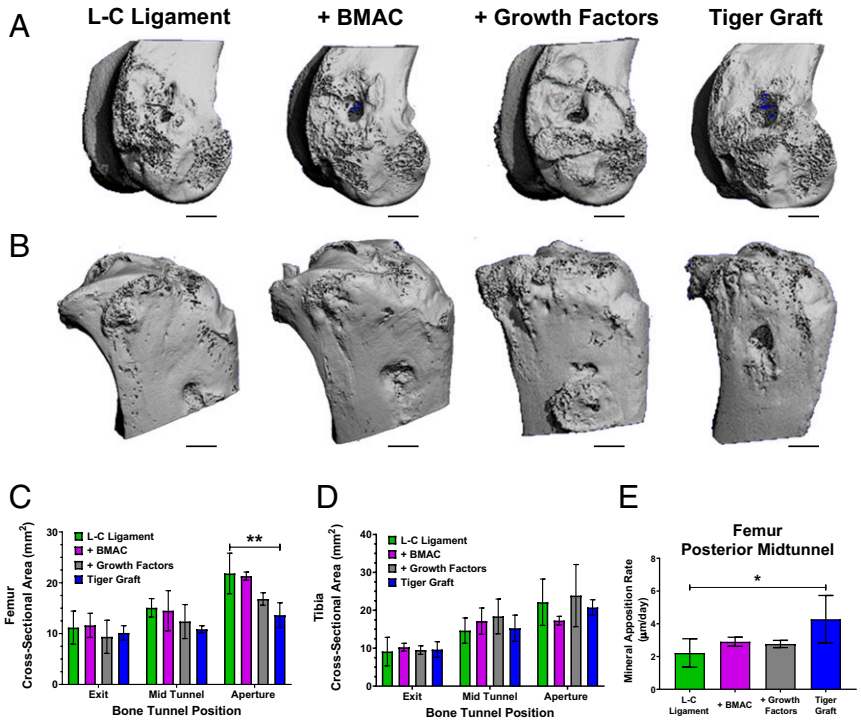

Fig. 7. Incorporation of PET fibers in the bioengineered ACL matrix enhances osteointegration and decreases bone tunnel cross-sectional area via increased mineral apposition rate. (*A*) Representative μCT images of rabbit femur ($n = 3$, 12 wk post-ACL reconstruction). (Scale bars, 3 mm.) (*B*) Representative μCT images of rabbit tibia ($n = 3$, 12 wk post-ACL reconstruction). (Scale bars, 3 mm.) (*C*) Quantification of bone tunnel cross-sectional area at various segments of the femoral bone tunnel. Mean cross-sectional area ± SD ($n = 2$ to 3, 12 wk post-ACL reconstruction); $^{**}P = 0.0097$, one-way ANOVA with Dunnett's multiple-comparisons test. (*D*) Quantification of bone tunnel cross-sectional area at various segments of the tibial bone tunnel. Mean cross-sectional area ± SD ($n = 3$, 12 wk post-ACL reconstruction); no significant difference between groups, one-way ANOVA with Dunnett's post hoc test. (*E*) Quantification of the femoral mineral apposition rate in the posterior midtunnel area. Mean mineral apposition rate ± SD ($n = 3$, 12 wk post-ACL reconstruction). $^{*}P = 0.0466$, one-way ANOVA with Dunnett's post hoc test.

BMAC for grade 1, 2, and 3 ACL tears, and found an improvement in ACL integrity in 7 of 10 patients based on postprocedural MRIs. However, no randomized controlled clinical trials have been completed (to our knowledge) on the use of BMAC treatment in conjunction with ACL reconstruction. Animal studies have investigated the ability of mesenchymal stem cells, which were expanded in vitro, to stimulate osteointegration of tendon grafts. They found that MSCs promote direct tendon-to-bone healing, and thus the presence of chondrocytes at the interface (19, 50). However, no animal studies have reported the use of autologous BMAC for ACL reconstruction. This report demonstrates the feasibility of concentrating BMA intraoperatively. Aside from the histological observations, we also observed a trend toward a less inflammatory synovial fluid profile with the use of BMAC. These findings suggest that BMAC therapy may be an effective strategy to accelerate the regeneration of the ACL.

BMP-2 Delivery Was Not Found to Significantly Effect Bone Formation. As an osteoinductive agent, we hypothesized that BMP-2 would induce osteoblast differentiation and subsequent bone formation, and a dose of 10 μg was chosen based on studies that demonstrated induction of bone formation with similar doses in a fibrin gel (21). Thus, it was expected that supplementation with BMP-2 in a fibrin gel carrier would induce greater bone formation, but this was not consistently observed. The 3D reconstruction of μCT data demonstrated increased orthotopic bone formation in only a few cases (Fig. 7 *A* and *B*) and robust bone ingrowth in one case (Fig. 5 *A*, *iii*). Future studies should consider a systematic investigation of the effect of higher doses of BMP-2 in a fibrin gel matrix to enhance bone regeneration in a rabbit ACL reconstruction model.

Intraarticular Application of FGF-2 and FGF-8 May Inhibit Adipogenesis, Leading to Decreased Joint Space Inflammation. In this study, we found that intraarticular treatment with FGF-2 and FGF-8 significantly down-regulated leptin production (Fig. 6*F*). Moreover, we found a strong direct correlation between leptin production and levels of several proinflammatory cytokines (Fig. 6*I* and *SI Appendix*, Fig. S3). In contrast, we observed an inverse relationship was found between leptin and antiinflammatory cytokines (Fig. 6*J* and *SI Appendix*, Fig. S3). Recently, Westphal et al. (51) demonstrated that FGF-8 inhibits adipogenesis. Thus, we hypothesize that the application of FGF-8 in this study may have inhibited adipogenesis in the knee leading to the reduced inflammatory synovial fluid profile observed.

Increasing evidence suggests that leptin, a hormone secreted by adipocytes, plays a role in the pathogenesis of osteoarthritis by stimulating an inflammatory environment in the knee (52). In the knee joint, the major source of adipocytes is the infrapatellar (or Hoffa's) fat pad (52). It has been suggested that leptin increases the production of proinflammatory cytokines, IL-8 and IL-6, through binding to the leptin receptor on synovial fibroblasts (53, 54). A correlation between high body mass index and increased incidence of osteoarthritis in non–weight-bearing joints has also been reported, suggesting that increased body mass index also has a nonmechanical contribution to the pathogenesis of osteoarthritis (55). Although some data indicate that leptin can produce anabolic effects on cartilage, an abundance of evidence implicates leptin in inflammation and osteoarthritis (55).

The tiger graft and L-C ligament were found to have similar cytokine profiles at 12 wk. Previous research with ACL prostheses fabricated entirely with PET did not exhibit regeneration of ACL tissue and failed due to material fatigue and reactive synovitis caused by PET wear particles (6, 56). In this study, robust tissue regeneration was found within the tiger graft, and this may have shielded the PET fibers from generating wear particles that can lead to an inflammatory process. Future studies will need to investigate the synovial fluid cytokine profile between the L-C ligament and tiger graft at later time points.

Mechanical and Chemical Properties of the Tiger Graft May Enhance Osteointegration. A significantly higher mineral apposition rate and reduced bone tunnel cross-sectional area was found in the tiger graft group compared to the L-C ligament. The incorporation of nondegradable PET in the tiger graft caused an increase in its biomechanical properties compared to the L-C ligament at 12 wk

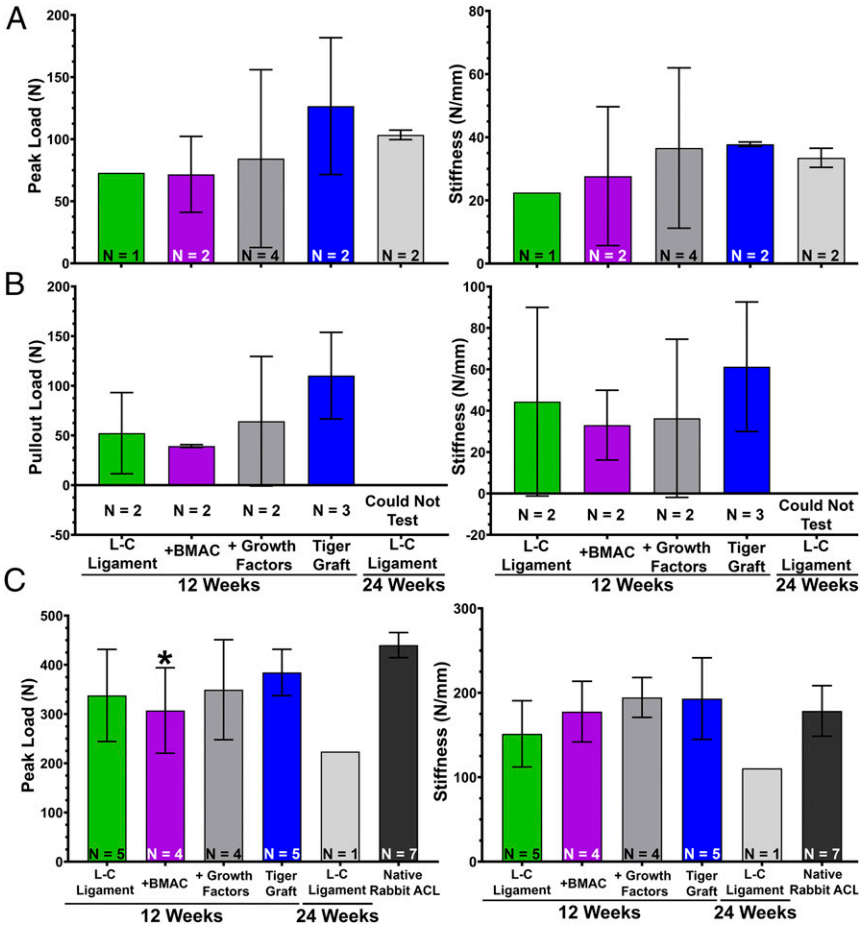

Fig. 8. Incorporation of PET fibers into the bioengineered ACL matrix exhibits enhanced mechanical properties at 12 wk and is comparable to the native rabbit ACL. (*A*) Quantification of peak load (*Left*) and stiffness (*Right*) of primary midsubstance ruptures. Mean peak load and stiffness ± SD (sample size indicated in panel). (*B*) Quantification of bone tunnel pull-out load (*Left*) and stiffness (*Right*) of the bioengineered ACL matrices. Mean pull-out load and stiffness ± SD (sample size indicated in panel). (*C*) Quantification of peak load (*Left*) and stiffness (*Right*) of secondary midsubstance ruptures. Mean peak load and stiffness ± SD (sample size indicated in panel); $*P < 0.05$, one-way ANOVA with Dunnett's post hoc test with native rabbit ACL as the control.

(Fig. 8). Therefore, we hypothesize that the tiger graft exerted greater forces than the L-C ligament within the bone tunnel, leading to the increased mineral apposition rate. During normal ambulation, compressive forces are likely placed on the bone as the bioengineered ACL matrix presses on the matrix–bone interface. Given the kinematics of the knee, the posterior bone tunnel likely experiences the greatest compressive forces. Interestingly, we observed that the mineral apposition rate was highest in the posterior bone tunnel (Fig. 7*E*). Several other studies have demonstrated that the application of compressive forces on bone enhances the mineral apposition rate (57, 58). Furthermore, our reported mineral apposition rates are in agreement with other studies conducted in rabbit models (57). In future studies, the application of controlled loading could be used to determine the causal relationship between mechanical loading and bone regeneration during ACL reconstruction.

The degradation by-products of PLLA may contribute to a local acidic environment that inhibits bone mineralization. The tiger graft group is composed of 20 yarns of PLLA and 4 yarns of PET, 16.67% less PLLA than the L-C ligament. Our original hypothesis was that the PET would allow for strength retention of the bioengineered ACL matrix, which also held true as the tiger grafts at harvest exhibited fewer yarn ruptures. However, the finding that there is a trend toward higher mineral apposition rates throughout the bone tunnels of the femur and tibia was not expected. Mineralization of bone is thought to be governed by the activity of alkaline phosphatase (ALP), which is optimal at an alkaline pH (59). As PLLA degrades, acidic by-products are released, which may reduce ALP activity, and in turn, the measured mineral apposition rate (60). Studies have shown that slight pH changes can affect bone healing and mineralization (60–63), and in vitro degradation studies of PLLA scaffolds have shown detectable decreases in pH by 21 d (64, 65). Future studies will need to assess the effect of the L-C ligament and tiger graft on the local microenvironment pH of the synovial fluid and bone tunnel.

Tiger Graft Demonstrates Enhanced Mechanical Properties. The goal of a bioengineered ACL matrix for ACL reconstruction is to serve as a mechanically competent scaffold that gradually transfers the loads experienced by the knee to newly regenerated tissue. This is achieved by facilitating tissue regeneration in an organized fashion. We previously demonstrated that the bioengineered ACL matrix facilitates organized deposition of a nanofibrous extracellular matrix at 12 wk with scanning electron microscopy (5). Furthermore, we previously showed that, at 12 wk, cellular infiltration and tissue deposition was achieved throughout the matrix thickness (4). In this study, histological analysis demonstrated robust soft tissue regeneration between the fibers of the bioengineered ACL matrix. Thus, the contribution of the regenerated soft tissue was expected to be represented in the biomechanical testing.

The mechanical contribution of soft tissue regeneration was best represented in the stiffness observed in secondary midsubstance ruptures (Fig. 8 *C*, *Right*). The L-C ligament and tiger graft had a stiffness around 30 N/mm at the time of implantation (*SI Appendix*, Fig. S6*C*). At 12 wk postimplantation, approximately a fivefold increase in the stiffness was found and the bioengineered ACL matrices had statistically similar stiffness compared to the native rabbit ACL. This increased stiffness is likely due to the soft tissue regeneration within the bioengineered ACL matrix and its adhesion to the PLLA and PET fibers.

Another goal of this study was to enhance the osteointegration of the bioengineered ACL matrix to the point of superseding the strength of mechanical fixation provided by the titanium suture buttons and fiberloop. Our findings demonstrate that suture fixation is still the weakest link of the bioengineered ACL matrix complex at 12 wk. Given our methodology, biomechanical testing without removing the titanium suture buttons, our conclusions on the strength of osteointegration are limited. Nevertheless, a trend toward greater osteointegration was seen in the tiger graft group (Fig. 8*B*). This result, in combination with the reduced bone tunnel size and enhanced mineral apposition rate seen with the tiger graft, suggests that the combination of PLLA and PET led to enhanced osteointegration in comparison to the L-C ligament. Moreover, the pull-out loads in the present study are similar to other investigations into the strength of osteointegration with tendon autografts and allografts in rabbit models (30, 66). Studies using matrices composed of PET also resulted in pull-out loads between 45 and 53 N (67, 68). Considering the initial loads placed on the bioengineered ACL matrices prior to testing for the bone tunnel pull-out load, the results regarding osteointegration strength are promising. Future studies should investigate the true pull-out load of the bioengineered ACL matrix by removing the titanium suture buttons prior to tensile tests.

The bioengineered ACL matrix demonstrated similar peak loads at 12 wk to the native rabbit ACL. An initial loss in the strength of ACL autografts and allografts after ACL reconstruction has been established, and the same trend was seen with the bioengineered ACL matrices. At 12 wk, the L-C ligament exhibited a strength retention of 34% in comparison to day 0. The strength retention of the tiger graft was 39.4%. However, the bioengineered ACL matrix was designed to compensate for this predicted loss in strength. Thus, the finding that the peak loads of the bioengineered ACL matrices at 12 wk was comparable to the native rabbit ACL demonstrated the success of the design to account for the expected loss of strength. In comparison to other rabbit ACL reconstructions that resulted in midsubstance ruptures of autografts and synthetic ligaments, the peak loads reported in the present study were generally threefold greater (4, 30, 31).

Limitations. There are a few limitations in this study. First, rabbits are quadrupeds that have a higher degree of flexion at rest, which causes distinctly different biomechanics compared to the human knee. Second, the relatively small sample size increases the risk of bias. Finally, long-term evaluations of BMAC treatment and the tiger graft are needed to answer whether 1) the change in cellular phenotype and extracellular matrix seen with BMAC treatment result in enhanced endochondral ossification within the bone tunnels at longer times points; 2) the strength retention of the tiger graft remains superior to the L-C ligament at 24 wk.

Conclusions

We have conducted a comparative analysis of the effects of biological factors and material composition on the outcome of ACL reconstruction with a bioengineered ACL matrix. Treatment with BMAC showed the ability to increase cuboidal cellular phenotypes reminiscent of ACL fibroblasts and chondrocyte-like cells. Growth factor treatment resulted in the down-regulation of inflammatory markers. Overall, this study demonstrates that material composition strongly influences the tissue regeneration and biomechanical performance of the bioengineered ACL matrix. The combination of PLLA and PET in the tiger graft should be further explored in a preclinical large-animal model.

Materials and Methods

Study Design. The objective of this study was to conduct a comparative analysis on the effect of bioengineered ACL matrix material composition and bioactive factors toward its regeneration and functional outcomes in a rabbit ACL reconstruction model. This study was a randomized, nonblinded, and controlled laboratory experiment. Bioengineered ACL matrices were fabricated using a custom-made 3D braiding machine (29). Animal experiments were approved by the Institutional Animal Care and Use Committee, University of Connecticut Health. Forty-four New Zealand White rabbits (7 to 8 mo, 3 to 4 kg) were used in this study and were divided into four groups (n = 11, each) for 12 wk: 1) L-C ligament, 2) L-C ligament + BMAC, 3) L-C ligament + growth factors, and 4) tiger graft. Eleven additional animals received the L-C ligament and were harvested at 24 wk. Based on a power analysis (β = 80%, α = 5%), eight animals were designated for mechanical testing and three animals for histology. Synovial fluid analysis was conducted (n = 3–11), based on sample availability. The L-C ligament and tiger graft groups received fibrin glue to serve as a carrier control, and the fibrin glue was delivered to three locations: the extracortical exit of the tibia, the extracortical exit of the femur, and the intraarticular space. Fibrin glue served as a carrier for the application of BMAC and growth factors. Animals in the BMAC treatment group received BMAC in all three locations. The following growth factors were administered in the growth factors treatment group: 1) 10 μg of BMP-2 was delivered to the extracortical exits of the femur and tibia (Fig. 1*D*), and 2) 100 ng of FGF-2 and 100 ng of FGF-8b mixed were delivered to the intraarticular space (Fig. 1*C*).

Statistical Analysis. All data are reported as means ± SD. Fisher's exact t test was used to analyze contingency tables. A normality test was run for all of the data. For comparison between multiple groups, one-way ANOVA test was used with Dunnett's multiple comparisons in which the L-C ligament or native rabbit ACL served as the control. A Kruskal–Wallis test was run to compare multiple groups if the data failed the test for normality. For BMA and BMAC comparison, the Wilcoxon test was used because the samples did not pass a test for normality and were paired observations. Cytokine data did not pass the normality test; thus, a Kruskal–Wallis test (nonparametric one-way ANOVA) was used. The μCT and mineral apposition rate data passed the normality test; therefore, a one-way ANOVA with Dunnett's multiple comparisons was used in which the L-C ligament served as the control. An unpaired t test was used to analyze two groups when the data passed the normality test. A Mann–Whitney test was used to analyze two groups when the data did not pass the normality test. GraphPad Prism 8 was used for all analysis.

Data Availability. All study data are included in the article and *SI Appendix*.

ACKNOWLEDGMENTS. We thank the Center for Comparative Medicine and Flow Cytometry Core at the University of Connecticut Health. We thank Dr. Stephen Doty for his assistance in histology. We thank Rong Wu for her assistance with statistical analysis. This research was supported by funding from the Raymond and Beverly Sackler Center for Biomedical, Biological, Physical and Engineering Sciences, NIH Grant R01AR063698, and NIH Grant DP1AR068147. P.Y.M. was supported by the NIH Supplemental Grant to Promote Diversity in Health-Related Research Program (NIH Grant R01AR063698-02S1). Suture materials, titanium buttons, dual syringe kit, and drill bits were donated by Arthrex.

1. M. V. Paterno, M. J. Rauh, L. C. Schmitt, K. R. Ford, T. E. Hewett, Incidence of second ACL injuries 2 years after primary ACL reconstruction and return to sport. *Am. J. Sports Med.* **42**, 1567–1573 (2014).
2. J. D. Harris *et al.*, Return-to-sport and performance after anterior cruciate ligament reconstruction in national basketball association players. *Sports Health* **5**, 562–568 (2013).
3. V. M. Shah, J. R. Andrews, G. S. Fleisig, C. S. McMichael, L. J. Lemak, Return to play after anterior cruciate ligament reconstruction in National Football League athletes. *Am. J. Sports Med.* **38**, 2233–2239 (2010).
4. J. A. Cooper Jr *et al.*, Biomimetic tissue-engineered anterior cruciate ligament replacement. *Proc. Natl. Acad. Sci. U.S.A.* **104**, 3049–3054 (2007).
5. P. Y. Mengsteab *et al.*, Evaluation of a bioengineered ACL matrix's osteointegration with BMP-2 supplementation. *PLoS One* **15**, e0227181 (2020).
6. P. Y. Mengsteab, L. S. Nair, C. T. Laurencin, The past, present and future of ligament regenerative engineering. *Regen. Med.* **11**, 871–881 (2016).
7. M. A. Barajaa, L. S. Nair, C. T. Laurencin, Bioinspired scaffold designs for regenerating musculoskeletal tissue interfaces. *Regen. Eng. Transl. Med.*, 10.1007/s40883-019-00132-3 (2019).
8. C. T. Laurencin, A. McClinton, Regenerative cell-based therapies: Cutting edge, bleeding edge, and off the edge. *Regen. Eng. Transl. Med.* **6**, 78–89 (2020).
9. X. Yu, P. Y. Mengsteab, G. Narayanan, L. S. Nair, C. T. Laurencin, Enhancing the surface properties of a bioengineered anterior cruciate ligament matrix for use with point-of-care stem cell therapy. *Engineering*, 10.1016/j.eng.2020.02.010 (2020).
10. X. N. Liu *et al.*, Enhanced tendon-to-bone healing of chronic rotator cuff tears by bone marrow aspirate concentrate in a rabbit model. *Clin. Orthop. Surg.* **10**, 99–110 (2018).

11. M. Koch *et al*., Bone marrow aspirate concentrate for the treatment of avascular meniscus tears in a one-step procedure—evaluation of an in vivo model. *Int. J. Mol. Sci.* **20**, 1120 (2019).
12. S. Font Tellado, E. R. Balmayor, M. Van Griensven, Strategies to engineer tendon/ligament-to-bone interface: Biomaterials, cells and growth factors. *Adv. Drug Deliv. Rev.* **94**, 126–140 (2015).
13. D. Kobayashi, M. Kurosaka, S. Yoshiya, K. Mizuno, Effect of basic fibroblast growth factor on the healing of defects in the canine anterior cruciate ligament. *Knee Surg. Sports Traumatol. Arthrosc.* **5**, 189–194 (1997).
14. M. C. Hochberg *et al*., Effect of intra-articular sprifermin vs placebo on femorotibial joint cartilage thickness in patients with osteoarthritis: The FORWARD randomized clinical trial. *J. Am. Med. Assoc.* **322**, 1360–1370 (2019).
15. A. Makanae, K. Mitogawa, A. Satoh, Co-operative Bmp- and Fgf-signaling inputs convert skin wound healing to limb formation in urodele amphibians. *Dev. Biol.* **396**, 57–66 (2014).
16. S. A. Rodeo, K. Suzuki, X. H. Deng, J. Wozney, R. F. Warren, Use of recombinant human bone morphogenetic protein-2 to enhance tendon healing in a bone tunnel. *Am. J. Sports Med.* **27**, 476–488 (1999).
17. T. W. Axelrad, T. A. Einhorn, Bone morphogenetic proteins in orthopaedic surgery. *Cytokine Growth Factor Rev.* **20**, 481–488 (2009).
18. O. C. Ifegwu *et al*., Bone regenerative engineering using a protein kinase A-specific cyclic AMP analogue administered for short term. *Regen. Eng. Transl. Med.* **4**, 206–215 (2018).
19. M. Y. H. Soon, A. Hassan, J. H. P. Hui, J. C. H. Goh, E. H. Lee, An analysis of soft tissue allograft anterior cruciate ligament reconstruction in a rabbit model: A short-term study of the use of mesenchymal stem cells to enhance tendon osteointegration. *Am. J. Sports Med.* **35**, 962–971 (2007).
20. Y. Dong, Q. Zhang, Y. Li, J. Jiang, S. Chen, Enhancement of tendon-bone healing for anterior cruciate ligament (ACL) reconstruction using bone marrow-derived mesenchymal stem cells infected with BMP-2. *Int. J. Mol. Sci.* **13**, 13605–13620 (2012).
21. M. Kaipel *et al*., BMP-2 but not VEGF or PDGF in fibrin matrix supports bone healing in a delayed-union rat model. *J. Orthop. Res.* **30**, 1563–1569 (2012).
22. E. M. Moore, J. L. West, Bioactive poly(ethylene glycol) acrylate hydrogels for regenerative engineering. *Regen. Eng. Transl. Med.* **5**, 167–179 (2019).
23. J. R. Clegg, M. E. Wechsler, N. A. Peppas, Vision for functionally decorated and molecularly imprinted polymers in regenerative engineering. *Regen. Eng. Transl. Med.* **3**, 166–175 (2017).
24. S. Ben Abdessalem, F. Debbabi, H. Jedda, S. Elmarzougui, S. Mokhtar, Tensile and knot performance of polyester braided sutures. *Text. Res. J.* **79**, 247–252 (2009).
25. L. S. Nair, C. T. Laurencin, M. T. Aronson, "Mechanically competent scaffold for ligament and tendon regeneration." US Patent US8758437B2 (2012).
26. M. Kapoor, J. Martel-Pelletier, D. Lajeunesse, J. P. Pelletier, H. Fahmi, Role of proinflammatory cytokines in the pathophysiology of osteoarthritis. *Nat. Rev. Rheumatol.* **7**, 33–42 (2011).
27. M. Maurer, E. von Stebut, Macrophage inflammatory protein-1. *Int. J. Biochem. Cell Biol.* **36**, 1882–1886 (2004).
28. S. M. Opal, V. A. DePalo, Anti-inflammatory cytokines. *Chest* **117**, 1162–1172 (2000).
29. P. Y. Mengsteab *et al*., Ligament regenerative engineering: Braiding scalable and tunable bioengineered ligaments using a bench-top braiding machine. *Regen. Eng. Transl. Med.*, 10.1007/s40883-020-00178-8 (2020).
30. X. M. Wang, G. Ji, X. M. Wang, H. J. Kang, F. Wang, Biological and biomechanical evaluation of autologous tendon combined with ligament advanced reinforcement system artificial ligament in a rabbit model of anterior cruciate ligament reconstruction. *Orthop. Surg.* **10**, 144–151 (2018).
31. M. Kosaka, J. Nakase, K. Hayashi, H. Tsuchiya, Adipose-derived regenerative cells promote tendon-bone healing in a rabbit model. *Arthroscopy* **32**, 851–859 (2016).
32. J. A. Cooper, H. H. Lu, F. K. Ko, J. W. Freeman, C. T. Laurencin, Fiber-based tissue-engineered scaffold for ligament replacement: Design considerations and in vitro evaluation. *Biomaterials* **26**, 1523–1532 (2005).
33. L. V. Gulotta, S. A. Rodeo, Biology of autograft and allograft healing in anterior cruciate ligament reconstruction. *Clin. Sports Med.* **26**, 509–524 (2007).
34. H. Fan, H. Liu, E. J. W. Wong, S. L. Toh, J. C. H. Goh, In vivo study of anterior cruciate ligament regeneration using mesenchymal stem cells and silk scaffold. *Biomaterials* **29**, 3324–3337 (2008).
35. W. Nebelung, R. Becker, D. Urbach, M. Röpke, A. Roessner, Histological findings of tendon-bone healing following anterior cruciate ligament reconstruction with hamstring grafts. *Arch. Orthop. Trauma Surg.* **123**, 158–163 (2003).
36. A. Bedi, S. Kawamura, L. Ying, S. A. Rodeo, Differences in tendon graft healing between the intra-articular and extra-articular ends of a bone tunnel. *HSS J.* **5**, 51–57 (2009).
37. T. Chen, P. Zhang, J. Chen, Y. Hua, S. Chen, Long-term outcomes of anterior cruciate ligament reconstruction using either synthetics with remnant preservation or hamstring autografts: A 10-year longitudinal study. *Am. J. Sports Med.* **45**, 2739–2750 (2017).
38. V. B. Duthon *et al*., Anatomy of the anterior cruciate ligament. *Knee Surg. Sports Traumatol. Arthrosc.* **14**, 204–213 (2006).
39. J. Zhu, X. Zhang, Y. Ma, C. Zhou, Y. Ao, Ultrastructural and morphological characteristics of human anterior cruciate ligament and hamstring tendons. *Anat. Rec. (Hoboken)* **295**, 1430–1436 (2012).
40. G. Pattappa, J. Zellner, B. Johnstone, D. Docheva, P. Angele, Cells under pressure—the relationship between hydrostatic pressure and mesenchymal stem cell chondrogenesis. *Eur. Cell. Mater.* **37**, 360–381 (2019).
41. J. W. Freeman, M. D. Woods, C. T. Laurencin, Tissue engineering of the anterior cruciate ligament using a braid-twist scaffold design. *J. Biomech.* **40**, 2029–2036 (2007).
42. N. Saveh-Shemshaki, L. S Nair, C. T. Laurencin, Nanofiber-based matrices for rotator cuff regenerative engineering. *Acta Biomater.* **94**, 64–81 (2019).
43. W. Kusswetter, H. J. Refior, Microscopical and scanning electron microscopical findings in ligament insertions. *Z. Orthop. Ihre Grenzgeb.* **123**, 876–879 (1985).
44. F. Pauwels, Eine neue theorie über den einfluß mechanischer reize auf die differenzierung der stützgewebe–Zehnter beitrag zur funktionellen anatomie und kausalen morphologie des stützapparates. *Z. Anat. Entwicklungsgesch.* **121**, 478–515 (1960).
45. Y. S. Kim, H. J. Lee, J. H. Ok, J. S. Park, D. W. Kim, Survivorship of implanted bone marrow-derived mesenchymal stem cells in acute rotator cuff tear. *J. Shoulder Elbow Surg.* **22**, 1037–1045 (2013).
46. M. Vilalta *et al*., Biodistribution, long-term survival, and safety of human adipose tissue-derived mesenchymal stem cells transplanted in nude mice by high sensitivity non-invasive bioluminescence imaging. *Stem Cells Dev.* **17**, 993–1003 (2008).
47. A. I. Caplan, Adult mesenchymal stem cells for tissue engineering versus regenerative medicine. *J. Cell. Physiol.* **213**, 341–347 (2007).
48. J. Holton, M. Imam, J. Ward, M. Snow, The basic science of bone marrow aspirate concentrate in chondral injuries. *Orthop. Rev. (Pavia)* **8**, 6659 (2016).
49. C. J. Centeno, J. Pitts, H. Al-Sayegh, M. D. Freeman, Anterior cruciate ligament tears treated with percutaneous injection of autologous bone marrow nucleated cells: A case series. *J. Pain Res.* **8**, 437–447 (2015).
50. K. M. Jang, H. C. Lim, W. Y. Jung, S. W. Moon, J. H. Wang, Efficacy and safety of human umbilical cord blood-derived mesenchymal stem cells in anterior cruciate ligament reconstruction of a rabbit model: New strategy to enhance tendon graft healing. *Arthroscopy* **31**, 1530–1539 (2015).
51. S. Westphal *et al*., Fibroblast growth factor 8b induces uncoupling protein 1 expression in epididymal white preadipocytes. *Sci. Rep.* **9**, 8470 (2019).
52. Y. H. Gao *et al*., An update on the association between metabolic syndrome and osteoarthritis and on the potential role of leptin in osteoarthritis. *Cytokine* **129**, 155043 (2020).
53. W. H. Yang *et al*., Leptin induces IL-6 expression through OBRl receptor signaling pathway in human synovial fibroblasts. *PLoS One* **8**, e75551 (2013).
54. K. M. Tong *et al*., Leptin induces IL-8 expression via leptin receptor, IRS-1, PI3K, Akt cascade and promotion of NF-kappaB/p300 binding in human synovial fibroblasts. *Cell. Signal.* **20**, 1478–1488 (2008).
55. P. F. Hu, J. P. Bao, L. D. Wu, The emerging role of adipokines in osteoarthritis: A narrative review. *Mol. Biol. Rep.* **38**, 873–878 (2011).
56. P. Di Benedetto *et al*., Histological analysis of ACL reconstruction failures due to synthetic-ACL (LARS) ruptures. *Acta Biomed.* **91**, 136–145 (2020).
57. X. Yang *et al*., Trabecular bone adaptation to loading in a rabbit model is not magnitude-dependent. *J. Orthop. Res.* **31**, 930–934 (2013).
58. D. F. Xu, G. X. Qu, S. G. Yan, X. Z. Cai, Microbubble-mediated ultrasound outweighs low-intensity pulsed ultrasound on osteogenesis and neovascularization in a rabbit model of steroid-associated osteonecrosis. *BioMed Res. Int.* **2018**, 4606791 (2018).
59. H. Orimo, The mechanism of mineralization and the role of alkaline phosphatase in health and disease. *J. Nippon Med. Sch.* **77**, 4–12 (2010).
60. D. A. Chakkalakal, A. A. Mashoof, J. Novak, B. S. Strates, M. H. McGuire, Mineralization and pH relationships in healing skeletal defects grafted with demineralized bone matrix. *J. Biomed. Mater. Res.* **28**, 1439–1443 (1994).
61. W. Liu *et al*., Alkaline biodegradable implants for osteoporotic bone defects–Importance of microenvironment pH. *Osteoporos. Int.* **27**, 93–104 (2016).
62. W. Liu, X. Dan, W. W. Lu, H. Pan, *Importance of Biomaterials In Vivo Microenvironment pH (μe-pH) in the Regeneration Process of Osteoporotic Bone Defects* (Springer, Singapore, 2018), pp. 473–495.
63. J. C. Berkmann *et al*., Early pH changes in musculoskeletal tissues upon injury—Aerobic catabolic pathway activity linked to inter-individual differences in local pH. *Int. J. Mol. Sci.* **21**, 2513 (2020).
64. Y. S. Liu, Q. L. Huang, A. Kienzle, W. E. G. Müller, Q. L. Feng, In vitro degradation of porous PLLA/pearl powder composite scaffolds. *Mater. Sci. Eng. C* **38**, 227–234 (2014).
65. K. S. Ogueri, T. Jafari, J. L. Escobar Ivirico, C. T. Laurencin, Polymeric biomaterials for scaffold-based bone regenerative engineering. *Regen. Eng. Transl. Med.* **5**, 128–154 (2019).
66. R. Wang, B. Xu, H. G. Xu, Up-regulation of TGF-β promotes tendon-to-bone healing after anterior cruciate ligament reconstruction using bone marrow-derived mesenchymal stem cells through the TGF-β/MAPK signaling pathway in a New Zealand white rabbit model. *Cell. Physiol. Biochem.* **41**, 213–226 (2017).
67. S. Wang *et al*., Enhance the biocompatibility and osseointegration of polyethylene terephthalate ligament by plasma spraying with hydroxyapatite in vitro and in vivo. *Int. J. Nanomedicine* **13**, 3609–3623 (2018).
68. C. Ai *et al*., Surface modification of vascular endothelial growth factor-loaded silk fibroin to improve biological performance of ultra-high-molecular-weight polyethylene via promoting angiogenesis. *Int. J. Nanomedicine* **12**, 7737–7750 (2017).